

SCIENTIFIC REPORTS

OPEN

Efficient Blue-emitting Phosphor $\text{SrLu}_2\text{O}_4:\text{Ce}^{3+}$ with High Thermal Stability for Near Ultraviolet (~400 nm) LED-Chip based White LEDs

Sheng Zhang^{1,2}, Zhendong Hao¹, Liangliang Zhang¹, Guo-Hui Pan¹, Huajun Wu¹, Xia Zhang¹, Yongshi Luo¹, Ligong Zhang¹, Haifeng Zhao¹ & Jiahua Zhang¹

Blue-emitting phosphors for near ultraviolet (NUV) based tri-color RGB phosphor blend converted white light emitting diodes (LEDs) have been extensively investigated in the past few years. LED chip peaked near 400 nm is the most efficient among the NUV chips currently. However, most of blue phosphors show inefficient excitation around 400 nm. Herein, a novel blue phosphor $\text{SrLu}_2\text{O}_4:\text{Ce}^{3+}$ matching well with near 400 nm chip and showing high thermal stability has been developed. The photoluminescence spectrum presents a broad emission band peaking at 460 nm with a bandwidth of nearly 90 nm. By optimizing the Ce^{3+} concentration, an internal quantum efficiency (IQE) as high as 76% was achieved. Furthermore, 86% of the room-temperature emission intensity is still maintained at 150 °C, indicating a good thermal stability and practicality. A series of white LEDs were fabricated based on 405 nm chips coated with a blend of the new blue phosphor with the commercial yellow and red phosphors. High color rendering indexes (≥ 90) were achieved while the correlated color temperature was tuneable in the range of 3094 to 8990 K. These results suggest that $\text{SrLu}_2\text{O}_4:\text{Ce}^{3+}$ can be utilized as a blue-emitting phosphor in NUV based white LEDs.

White LEDs have been widely deployed commercially on solid-state lighting, because of their superior efficiency and long life¹. Up to now, the most commonly used method to get white light based on monochrome LED is to combine a yellow-emitting phosphor such as cerium substituted yttrium aluminum garnet ($\text{Y}_3\text{Al}_5\text{O}_{12}:\text{Ce}^{3+}$) with a blue (InGa)N LED chip². However, the inconsistency of the aging characteristics of the blue chip and the phosphor can lead to the instability of the white light which is generated by the combination of the blue light from the chip and the yellow light from the phosphor. Furthermore, this type of white LED emits little red light and therefore has a low color rendering index^{3–8}. To resolve this problem, one can use an alternative method to obtain stable white light by a combination of a red-green-blue (RGB) phosphor blend with a near ultraviolet (NUV) LED chip^{9,10}. In this method, the visible components of the white light are generated only by phosphors, exhibiting low color point variation against the forward-bias currents. In the NUV chips, near 400 nm chip is more attractive because of the highest energy conversion efficiency. As a result, this approach requires all three RGB phosphors to have efficient excitation around 400 nm to maximize the device's efficiency.

Some blue-emitting phosphors as candidates for NUV (~400 nm) chip excitation have been reported, such as $\text{LiCaPO}_4:\text{Eu}^{2+}$ ¹¹, $\text{Ba}_3\text{LaNa}(\text{PO}_4)_3\text{F}:\text{Eu}^{2+}$ ¹², $\text{BaHfSi}_3\text{O}_9:\text{Eu}^{2+}$ ¹³, $\text{Ca}_2\text{LuScZrAl}_2\text{GeO}_{12}:\text{Ce}^{3+}$ ¹⁴, $\text{Ca}_3\text{Hf}_2\text{SiAl}_2\text{O}_{12}:\text{Ce}^{3+}$ ¹⁵, $\text{Ca}_3\text{Zr}_2\text{SiGa}_2\text{O}_{12}:\text{Ce}^{3+}$ ¹⁶, $\text{CaLaGa}_3\text{S}_6\text{O}:\text{Ce}^{3+}$ ¹⁷, $\text{Ca}_2\text{B}_5\text{O}_9\text{Br}:\text{Eu}^{2+}$ ¹⁸, and $\text{Na}_{3-2x}\text{Sc}_2(\text{PO}_4)_3:\text{xEu}^{2+}$ ¹⁹. But few of them could match well with near 400 nm chip and have high thermal stability at the same time. Therefore, it is essential to develop novel blue-emitting phosphors showing both excellent thermal stability and high quantum efficiency.

¹State Key Laboratory of Luminescence and Applications, Changchun Institute of Optics, Fine Mechanics and Physics, Chinese Academy of Sciences, 3888 Eastern South Lake Road, Changchun, 130033, China. ²University of Chinese Academy of Sciences, Beijing, 100049, China. Correspondence and requests for materials should be addressed to Z.H. (email: haozd@ciomp.ac.cn) or J.Z. (email: zhangjh@ciomp.ac.cn)

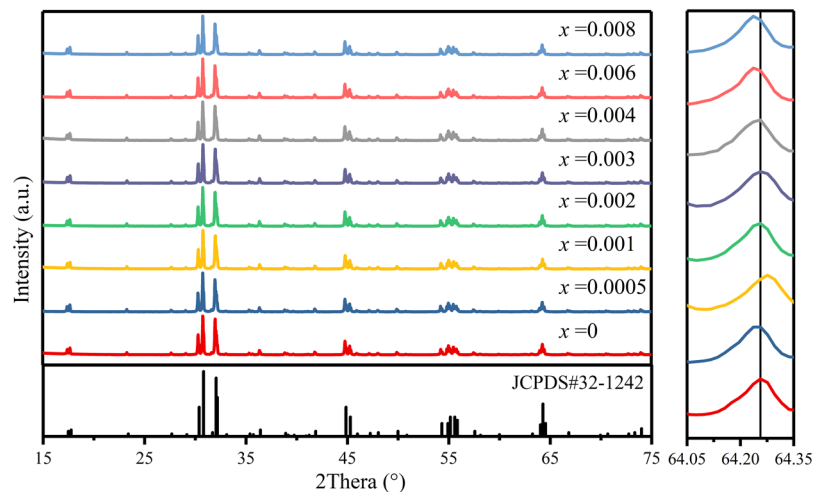


Figure 1. XRD patterns of prepared $\text{SrLu}_{2-x}\text{O}_4: x\text{Ce}^{3+}$ ($x = 0.0005\text{--}0.008$) phosphors. As a reference, the standard XRD pattern of SrLu_2O_4 (JCPDS No. 32-1242) is included. Right inset shows the peak shift of series XRD patterns with reference line locating at 64.2565° .

The rare-earth strontium oxides, SrLn_2O_4 (where $\text{Ln} = \text{Gd}, \text{Ho}, \text{Er}, \text{Tm}, \text{Yb}$), with the space group $Pn\bar{m}$ have been intensively studied for their magnetic properties^{20–22}. Selected SrLn_2O_4 as hosts, Eu^{3+} -doped SrLu_2O_4 and SrGd_2O_4 luminescent materials have been studied and considered as promising red phosphors in solid state lighting devices^{23,24}. Eu^{2+} doped SrLu_2O_4 exhibited a broad red emission centered at 610 nm, but it could be applied in optical temperature sensor instead of white LED because of its strong thermal quenching²⁵.

In this paper, we report to our knowledge for the first time, a novel blue phosphor of $\text{SrLu}_2\text{O}_4: \text{Ce}^{3+}$ prepared by solid state reaction. Photoluminescence (PL) properties and temperature dependence of the new phosphor are studied. The new phosphor shows efficient blue emission with the luminescence excitation band matching well with near 400 nm NUV chip. Besides, the phosphor also has high thermal stability with 86% of its room temperature emission intensity remained at 150 °C. White LEDs with high color rendering index (CRI) at different correlated color temperature (CCT) were fabricated based on NUV chips coated with blends of the new blue phosphor with the commercial yellow and red phosphors.

Results and Discussion

The phase purities and the crystal structures of the as-prepared powder samples $\text{SrLu}_{2-x}\text{O}_4: x\text{Ce}^{3+}$ ($x = 0.0005\text{--}0.008$) were characterized by XRD at room temperature. These samples all exhibit a single phase similar with the SrLu_2O_4 (JCPDS# 32-1242) crystal structure in Fig. 1. It is clearly that no new impurity appeared with the increasing concentration of Ce^{3+} . A slight shift of peak at 64.3° can be noticed. When x equals 0.01, peak shifts to bigger angle and it shifts to minor angle while x is more than 0.004. It can also be explained by Bragg equation:

$$2d\sin\theta = n\lambda \quad (1)$$

Peak shifting to minor angle means sites are occupied by bigger ions. In SrLu_2O_4 structure, the ion radius of Ce^{3+} (CN = 6, $r = 1.01 \text{ \AA}$; CN = 8, $r = 1.143 \text{ \AA}$) is between Sr^{2+} (CN = 8, $r = 1.26 \text{ \AA}$) and Lu^{3+} (CN = 6, $r = 0.861 \text{ \AA}$) which means it might take both sites. At low concentrations, Ce^{3+} tend to occupy Sr^{2+} sites. When x equals 0.01, Ce^{3+} occupied more Sr^{2+} than Lu^{3+} sites and represented shifting to bigger angle. While x is more than 0.004, Ce^{3+} occupied more Lu^{3+} than Sr^{2+} sites and represented shifting to minor angle. In this work, all the samples were synthesized based on the substitution of Ce^{3+} for Lu^{3+} by charge balance. However, it does not follow that the Ce^{3+} only occupies the Lu^{3+} site as mentioned above.

In order to further understand the microstructure of the as-prepared samples, detailed Rietveld refinements and lattice parameters are performed in Fig. 2(a) and Table 1. The crystal structure schematic diagram of SrLu_2O_4 is obtained according to the JCPDS cord using Diamond software, shown in Fig. 2(b). The Sr site is 8-coordinated with average Sr-O bond length of 2.6145 Å, while Lu site is 6-coordinated with average Lu-O bond length of 2.2917 Å.

Figure 3(a) and (b) show the SEM images of $\text{SrLu}_2\text{O}_4: 0.2\% \text{Ce}^{3+}$ unwashed and washed, respectively. It can be seen that small particles were washed away by alcohol and the particle was about 3 μm. Figures 3(c,d) show the micrographs of $\text{SrLu}_2\text{O}_4: 0.2\% \text{Ce}^{3+}$ phosphors under bright field light and 405-nm excitation, respectively. The size of particles in micrographs agrees with those in SEM images.

Figure 4(a) shows the normalized PLE ($\lambda_{\text{em}} = 460 \text{ nm}$) and PL ($\lambda_{\text{ex}} = 390 \text{ nm}$) spectra of $\text{SrLu}_2\text{O}_4: 0.2\% \text{Ce}^{3+}$ phosphors. The PLE spectrum of $\text{SrLu}_2\text{O}_4: \text{Ce}^{3+}$ in the UV region from 250 to 450 nm contains four distinctive bands peaked at 265 nm, 306 nm, 359 nm and 405 nm mainly ascribed to the allowed $4f\text{--}5d$ transitions of Ce^{3+} ²⁶. To obtain entire PL spectrum, we chose 390 nm as the excitation wavelength to avoid the effect of excitation light. The PL spectrum exhibits a strong blue emission peak at 460 nm with a full width at half maximum (FWHM) of approximately 90 nm. The asymmetric emission band can be well fitted with two Gaussian bands peaking at

Formula	SrLu ₂ O ₄
Temperature/K	300 K
Space group	<i>Pnam</i> (64)
Z	12
Lattice parameters	
a/Å	9.9747
b/Å	11.7482
c/Å	3.3395
V/Å ³	391.34
R _p /%	5.76
R _{wp} /%	6.35

Table 1. Rietveld refinement data of SrLu₂O₄.

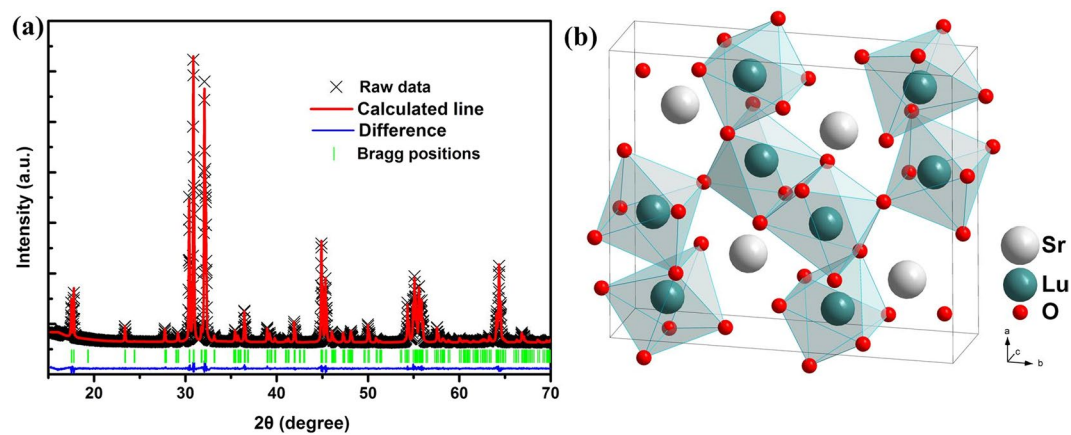


Figure 2. (a) Rietveld refinements for SrLu₂O₄. (b) Crystal structure schematic diagram of SrLu₂O₄.

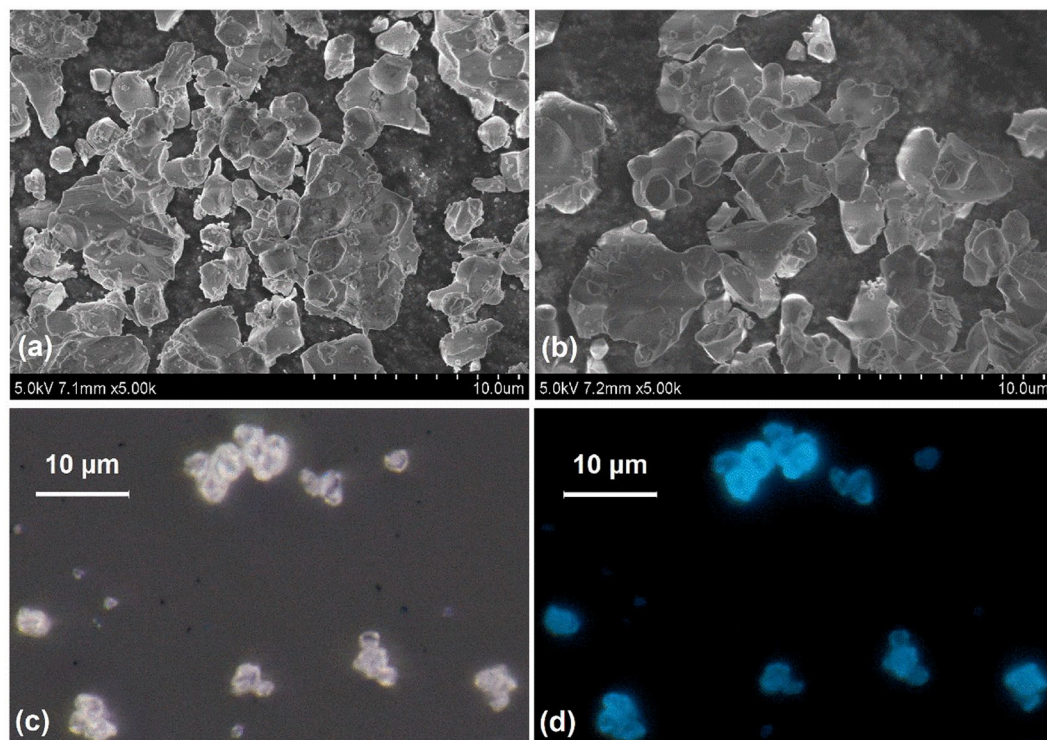


Figure 3. SEM images of SrLu₂O₄:Ce³⁺ phosphors unwashed (a) and washed (b). The photos of SrLu₂O₄:Ce³⁺ under fluorescence microscopy with bright field light (c) and 405 nm light (d) excitation.

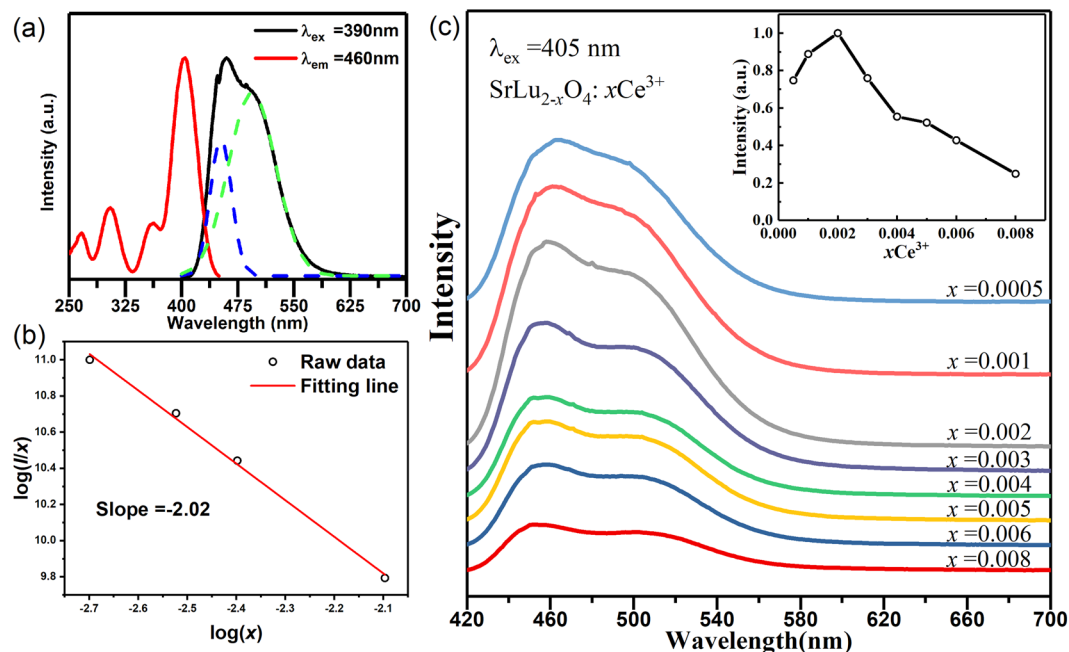


Figure 4. (a) PLE and PL spectra of SrLu_{1.998}O₄:0.002Ce³⁺ with the emission band fitted with two Gaussian curves (dashed). (b) Linear fitting of $\log(I/x)$ versus $\log(x)$ in the SrLu_{2-x}O₄:xCe³⁺ samples. (c) PL spectra of SrLu_{2-x}O₄:xCe³⁺ ($x = 0.0005$ - 0.008) under 405 nm excitation, the inset shows the dependence of integrated emission intensities on Ce³⁺ concentration.

20253 cm⁻¹ and 22165 cm⁻¹. Their energy difference is about 1912 cm⁻¹, being consistent with the energy separation between the ²F_{7/2} and the ²F_{5/2} sub-states of the ground state of Ce³⁺ (~2000 cm⁻¹)²⁷. IQEs were measured using a spectral on-coated integrating sphere and the measured results show that the IQE is 76.1%. The optimization of Ce³⁺ concentration in SrLu₂O₄ was performed by studying the PL spectra of SrLu_{2-x}O₄:xCe³⁺ for different Ce³⁺ concentrations ($x = 0.0005, 0.001, 0.002, 0.003, 0.004, 0.006$ and 0.008), as shown in Fig. 4(c). The concentration dependence of the PL intensities is depicted in the inset. It is clear that the maximal PL intensity occurs around 0.2% Ce³⁺. Further increasing Ce³⁺ concentration leads to PL decreasing due to the well-known concentration quenching effect. The concentration quenching originates from the larger probability of energy loss at a killer centre due to excitation energy migration among Ce³⁺ ions.

Here, the critical quenching distance (R_c), defined as an average distance between Ce³⁺ ions shorter than which luminescence quenching occurs, can be estimated from geometrical consideration by following formula^{5,28}:

$$R_c \approx 2 \left[\frac{3V}{4\pi X_c N} \right]^{1/3} \quad (2)$$

where V represents the volume of the unit cell, X_c represents the critical concentration of Ce³⁺ ions, and N represents the number of sites that can be replaced by Ce³⁺ in the unit cell. In this study, $V = 391.339 \text{ \AA}^3$, $N = 12$, and $X_c = 0.002$ for SrLu₂O₄:Ce³⁺. Thus, the R_c of Ce³⁺ ions were calculated to be 31.46 Å. The value is much larger than 5 Å, indicating that exchange interaction is not responsible and the electric multipolar–multipolar interaction should be suitable for the ET of this luminescence center²⁹.

The energy transfer mechanism among Ce³⁺ ions in this system is governed by electric multipolar interactions based on the Dexter theory. Furthermore, according to the report of Van Uitert the PL intensity and activator concentration satisfy the following equation³⁰:

$$\frac{I}{x} = \frac{k}{1 + \beta(x)^{1/\theta}} \quad (3)$$

where I is the PL intensity, x is the activator ion concentration, which is not less than the critical concentration, k and β are constants for a given host crystal under the same excitation conditions, and θ is an indication of the type of electric multipolar interactions. The value of θ is 6, 8, and 10, standing for the energy transfer mechanism of electric dipole-dipole, dipole-quadrupole, and quadrupole-quadrupole interactions, respectively. As shown in Fig. 4(b), the relationship of $\log(I/x)$ versus $\log(x)$ can be fitted linearly with a slope $-(\theta/3)$ equal to -2.02 . The value of θ is determined to be 6.06, which approximates to 6, implying that the concentration quenching of Ce³⁺ ions in the SrLu₂O₄:Ce³⁺ mainly results from the electric dipole-dipole interactions between Ce³⁺ ions. The large critical quenching distance might be explained as follows. Ce³⁺ ions may occupy Sr²⁺ and Lu³⁺ sites to form two luminescence centers (Ce1 and Ce2). We found that there was another emission band centered at 600 nm upon 480-nm excitation, as shown in Figures S1,S2. Here, we name the new band Ce2. One can observe that the PLE

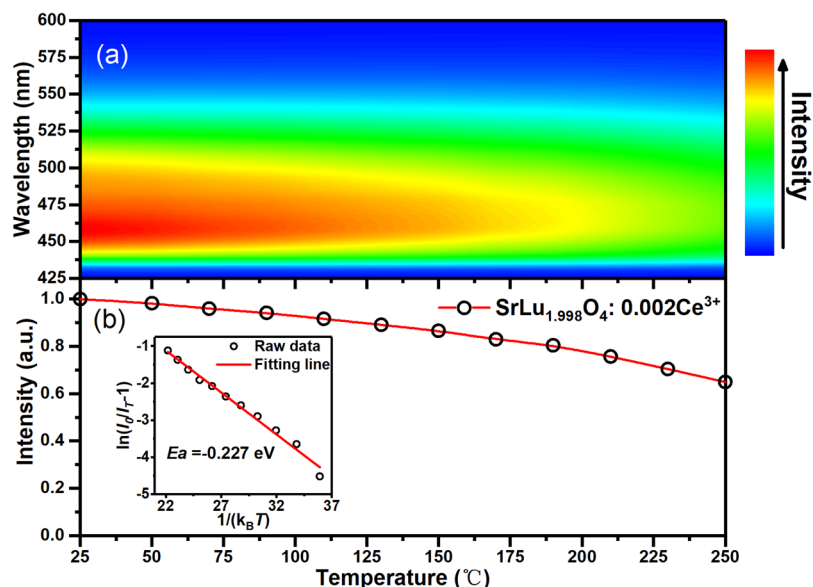


Figure 5. (a) Temperature-dependent measurement of the emission spectrum of $\text{SrLu}_{1.998}\text{O}_4:0.002\text{Ce}^{3+}$. (b) Temperature dependence of the integrated emission intensities in $\text{SrLu}_{1.998}\text{O}_4:0.002\text{Ce}^{3+}$ excited at 405 nm. The inset shows the Arrhenius fitting of the emission intensities.

Phosphor formula	$\lambda_{\text{ex}}/\text{nm}$	$\lambda_{\text{em}}/\text{nm}$	$I_{150^\circ\text{C}}$ (%)	$\Delta E/\text{eV}$	Ref.
$\text{SrLu}_2\text{O}_4:\text{Ce}^{3+}$	385-425	460	86	0.227	this work
$\text{Ca}_{5.45}\text{Li}_{3.55}(\text{SiO}_4)_3\text{O}_{0.45}\text{F}_{1.55}:\text{Ce}^{3+}$	330-420	470	71	0.27	4
$\text{Ca}_{1.65}\text{Sr}_{0.35}\text{SiO}_4:\text{Ce}^{3+}$	270-380	450	73	0.179	33
$\text{K}_2\text{ZrSi}_3\text{O}_9:\text{Eu}^{2+}$	380-420	465	35	0.304	34
$\text{YScSi}_4\text{N}_6:\text{Ce}^{3+}$	280-425	469	48	0.334	35
$\text{Ba}_7\text{Lu}_2\text{Si}_6\text{O}_{24}:\text{Eu}^{2+}$	250-420	460	39.6	0.341	36

Table 2. Comparison of luminescence properties of $\text{SrLu}_2\text{O}_4:\text{Ce}^{3+}$ and some existing blue phosphors. $I_{150^\circ\text{C}}$ denotes the luminescence intensity or QE at 150 °C relative to the value at RT.

band centered at 485 nm of Ce2 entirely overlaps with the PL band of Ce1, resulting in effective energy transfer from Ce1 to Ce2. The appearance of the strong Ce1 PLE band at 390 nm in the PLE spectrum of Ce2 is strong evidence for effective energy transfer. However, the Ce2 emission is too weak to be discernible compared to Ce1 center under 405-nm excitation at room temperature, as shown in Figure S3. This is because Ce2 is thermally quenched at room temperature. The detail study of luminescent properties of Ce2 is in progress. In this work, we lay emphasis on the optical properties of Ce1 center. The large critical distance for luminescence quenching of Ce1 is, therefore, attributed to effective energy transfer from Ce1 to Ce2.

The temperature-quenching property of $\text{SrLu}_{1.998}\text{O}_4:0.002\text{Ce}^{3+}$ was also studied. This new blue phosphor, $\text{SrLu}_{1.998}\text{O}_4:0.002\text{Ce}^{3+}$, shows a stability in the luminescence color. As shown in Fig. 5(a), a slight red shift and decrease in intensity can be observed with increasing temperature. In Fig. 5(b), the emitting intensity was up to 90% below 120 °C and still above 60% at 250 °C of that at room temperature (25 °C). It shows respectable thermostability and the luminescence properties of some recent blue phosphors are listed on Table 2. To better understand the temperature dependence of photoluminescence, the activation energy was calculated using the Arrhenius equation given as^{31,32}

$$I(T) = \frac{I_0}{1 + Ae^{-E_a/k_bT}} \quad (4)$$

where I_0 is the PL intensity at 0 K, here it is treated as the one at room temperature if the PL intensity is stable below room temperature, $I(T)$ is the PL intensity at a given temperature T , A is a constant, E_a is the activation energy for thermal quenching, and k_b is the Boltzmann constant. The experimental data are well fitted using Eq. (4), as shown in inset in Fig. 5(b). The value of E_a was obtained to be 0.227 eV for $\text{SrLu}_{1.998}\text{O}_4:0.002\text{Ce}^{3+}$. As the heat-treatment temperature increases, the thermal quenching of luminescence is usually attributed to a thermal activation process in which the excited electron energy is released preferentially through heat dissipation by phonons rather than radiation by photons.

Combined with $\text{SrLu}_2\text{O}_4:\text{Ce}^{3+}$ (blue), $(\text{Sr}, \text{Ba})_2\text{SiO}_4:\text{Eu}^{2+}$ (yellow) and $\text{Sr}_2\text{Si}_5\text{N}_8:\text{Eu}^{2+}$ (red) phosphors, the white LEDs based on NUV 405-nm chips have been fabricated and the digital images are shown in Fig. 6(a) and (b).

White LED	Weight ratio of constituents (%)			Ra	CCT (K)	η (lm/W)	CIE coordinates	
	blue	yellow	red				x	y
(c)	98.36	0.66	0.98	90.8	3094	16.51	0.4354	0.4125
(d)	98.52	0.49	0.99	91.2	4818	15.05	0.353	0.3774
(e)	98.93	0.25	0.82	90.0	8990	17.01	0.2783	0.3163
(f)	98.46	0.56	0.98	91.6	4393	36.77	0.3582	0.3343

Table 3. Performance parameters of four white LEDs under the current of 20 mA.

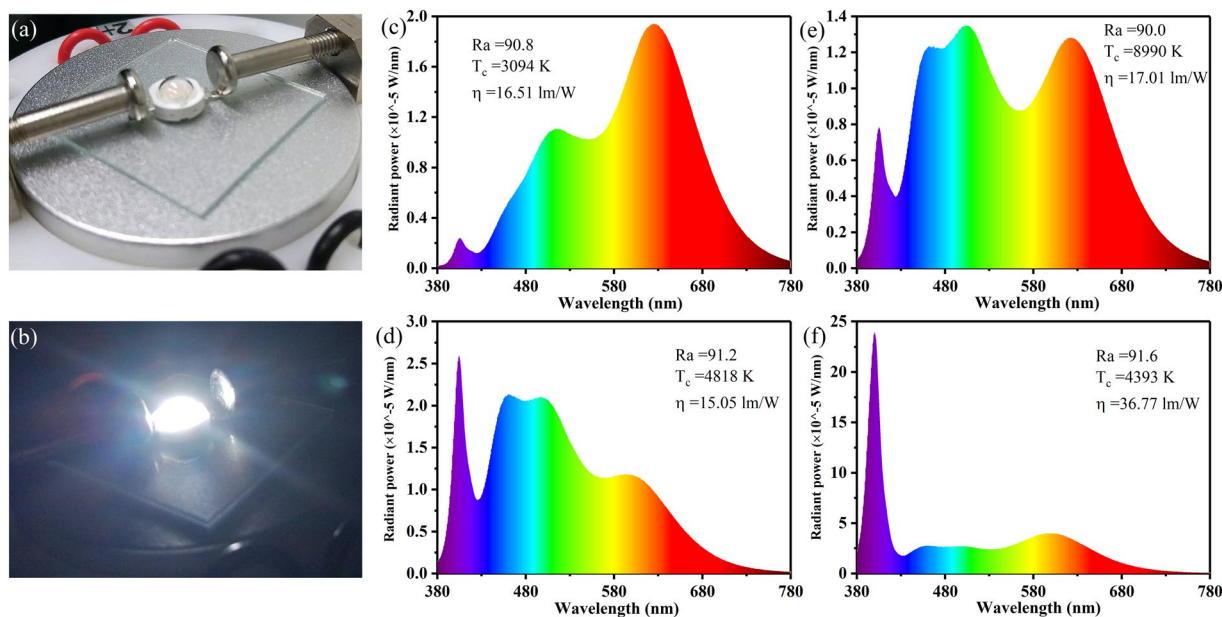


Figure 6. Digital images of the white LED unworked (a) and working under 20 mA and 3 V (b). (c–f) Emission spectra of white LEDs fabricated using NUV 405-nm chips combined with different ratios of $\text{SrLu}_2\text{O}_4:\text{Ce}^{3+}$ (blue), $(\text{Sr}, \text{Ba})_2\text{SiO}_4:\text{Eu}^{2+}$ (yellow) and $\text{Sr}_2\text{Si}_5\text{N}_8:\text{Eu}^{2+}$ (red) phosphors under a forward bias of 20 mA and 3 V.

Figure 6(c–f) show the electroluminescent spectra of fabricated white LED lamps with high color rendering index ($R_a \geq 90$). By changing different ratio of constituents, different correlated color temperature (CCT) can be achieved maintaining high R_a and the detailed parameters were listed in Table 3. White LEDs (c–e) were fabricated preliminarily to get high R_a and the luminous efficiency was overlooked. After fabrication optimization, considerably enhanced luminous efficiency of 36.77 lm/W with 91.6 R_a was achieved in white LED (f). The white LED luminous efficiency will be greatly improved in the future after fabricating conditions optimization in all aspects.

We chose $\text{SrLu}_{1-998}\text{O}_4:0.002\text{Ce}^{3+}$, commercial blue phosphor BAM and fabricated white LEDs (c, f) to carry on the conventional high temperature/high humidity (85 C/85RH) tests to prove its reliability. As shown in Fig. 7, white LEDs showed a great stable locating at 1.0 while both SLO and BAM phosphors fluctuated around 1.0 and SLO was better. Another group of fabricated white LEDs with near 40 lm/W were acquired and carried on the reliability test in Figures S4,S5, which also show great reliability.

All these results indicate that $\text{SrLu}_2\text{O}_4:\text{Ce}^{3+}$ phosphors have promising applications for white-light NUV LEDs.

Conclusions

The Ce^{3+} doped SrLu_2O_4 phosphor was synthesized via high-temperature solid-state reaction method. The XRD patterns indicated the purity of the crystal phase for the as-prepared samples. Under UV excitation at 405 nm, the PL spectrum of $\text{SrLu}_{1-998}\text{O}_4:0.002\text{Ce}^{3+}$ sample exhibits a broad blue emission band peaked at 460 nm with a high IQE of 76.1%. By changing the ratios of $\text{SrLu}_2\text{O}_4:\text{Ce}^{3+}$, yellow-emitting $(\text{Sr}, \text{Ba})_2\text{SiO}_4:\text{Eu}^{2+}$, and red-emitting $\text{Sr}_2\text{Si}_5\text{N}_8:\text{Eu}^{2+}$ phosphors, a series of white NUV LEDs with excellent color rendering index ($R_a \geq 90$) could be fabricated, and the correlated color temperatures were 3094 K, 4393 K, 4818 K and 8990 K, respectively. All results indicate that $\text{SrLu}_2\text{O}_4:\text{Ce}^{3+}$ can be promisingly used as an ultraviolet-convertible blue-emitting phosphor.

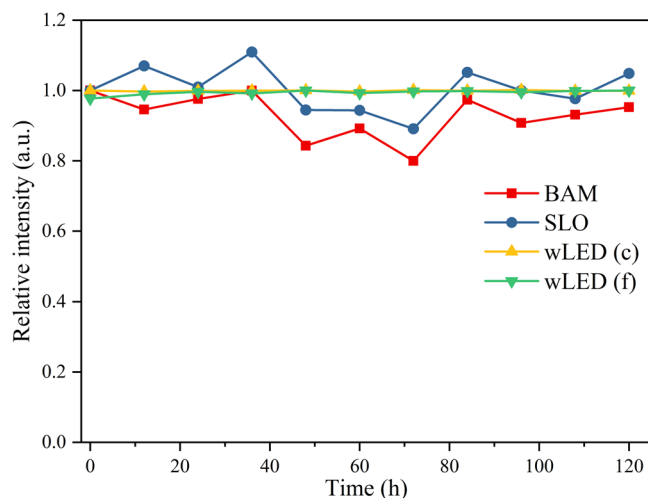


Figure 7. Relative integrated intensity of powder phosphors and fabricated white LEDs as a function of time: at temperature of 85 °C, in humidity at 85% RH.

Methods

Materials Synthesis. $\text{SrLu}_2\text{O}_4:\text{Ce}^{3+}$ samples were synthesized by traditional high-temperature solid-state reaction. The constituent oxides and carbonates, Sr_2CO_3 (A.R.), Lu_2O_3 (99.99%), CeO_2 (99.99%) were employed as the raw materials. The stoichiometric weighed powder according to the formula of $\text{SrLu}_{2-x}\text{O}_4:x\text{Ce}^{3+}$ was mixed in an agate mortar and placed in an alumina crucible. This crucible was heated at 1600 °C for 6 hours in a reducing atmosphere (95% N_2 /5% H_2), to reduce Ce^{4+} to Ce^{3+} . After sintering, the powders were furnace-cooled naturally down to room temperature (RT). Finally, the as-prepared powders were washed with alcohol three times and dried at 60 °C for 6 hours in a drying oven to obtain final phosphors. The NUV 405-nm chips we used were produced by Guangsheng Semiconductor Technology Co., Ltd. (chip size is 1.143 mm \times 1.143 mm and efficiency is 40%)

Characterization. X-ray diffraction (XRD) patterns were performed by a powder diffractometer (Bruker, D8 Focus, Cu $\text{K}\alpha$, 40 kV, 40 mA). The XRD data were collected in range of 15 to 75 degree (2θ) with count time of 2 s/step. The PL and photoluminescence excitation (PLE) spectra of Ce^{3+} were measured by FL900 fluorometer with a Xenon lamp (Edinburg Instruments, UK). The fluorescence micrographs and temperature-dependent PL spectra were carried out on a fluorescence microscopy (Olympus, BX53M). Internal quantum efficiency (IQE), i.e. the number ratio of the photon emitted to the photon absorbed, were measured directly by the absolute PL quantum yield measurement system (C9920-02, Hamamatsu Photonics K.K., Japan). The high temperature/high humidity (85 C/85RH) condition was provided by Programmable Temperature & Humidity Chamber (BPHJS-060A, China). The photoelectric properties of the fabricated white LEDs were measured by HAAS 2000 photoelectric measuring system (380 nm–780 nm, EVERFINE, China). The forward bias current was 20 mA. All the measurements were conducted at room temperature unless mentioned specially.

References

- Heber, J. Nobel Prize 2014: Akasaki, Amano & Nakamura (2014).
- Li, G. & Lin, J. Recent progress in low-voltage cathodoluminescent materials: synthesis, improvement and emission properties. *Chemical Society Reviews* **43**, 7099 (2014).
- Lee, S. P., Huang, C. H., Chan, T. S. & Chen, T. M. New Ce^{3+} -activated thiosilicate phosphor for LED lighting-synthesis, luminescence studies, and applications. *ACS Applied Materials & Interfaces* **6**, 7260 (2014).
- Zhou, J., Xia, Z., Yang, M. & Shen, K. High efficiency blue-emitting phosphor: Ce^{3+} -doped $\text{Ca}_{5.45}\text{Li}_{3.55}(\text{SiO}_4)_3\text{O}_{0.45}\text{F}_{1.55}$ for near UV-pumped light-emitting diodes. *Journal of Materials Chemistry* **22**, 21935, <https://doi.org/10.1039/c2jm34146h> (2012).
- Liu, Y. *et al.* An excellent cyan-emitting orthosilicate phosphor for NUV-pumped white LED application. *Journal of Materials Chemistry C* (2017).
- Wang, L. *et al.* $\text{Ca}_{1-x}\text{Li}_x\text{Al}_{1-x}\text{Si}_1+x\text{N}_3\text{Eu}^{2+}$ solid solutions as broadband, color-tunable and thermally robust red phosphors for superior color rendition white light-emitting diodes. *Light: Science & Applications* **5**, e16155, <https://doi.org/10.1038/lsa.2016.155> (2016).
- Dai, P. P. *et al.* A single Eu^{2+} -activated high-color-rendering oxychloride white-light phosphor for white-light-emitting diodes. *Light Science & Applications* **5**, e16024 (2016).
- Li, X. *et al.* New yellow $\text{Ba}_{0.93}\text{Eu}_{0.07}\text{Al}_2\text{O}_4$ phosphor for warm-white light-emitting diodes through single-emitting-center conversion. *Light Science & Applications* **2**, e50 (2013).
- Hao, Z. *et al.* White light emitting diode by using $\alpha\text{-Ca}_2\text{P}_2\text{O}_7:\text{Eu}^{2+}, \text{Mn}^{2+}$ phosphor. *Applied Physics Letters* **90**, 417–414 (2007).
- Zhang, Y., Xu, J., Cui, Q. & Yang, B. Eu^{3+} -doped $\text{Bi}_4\text{Si}_3\text{O}_{12}$ red phosphor for solid state lighting: microwave synthesis, characterization, photoluminescence properties and thermal quenching mechanisms. *Scientific Reports* **7**, 42464 (2017).
- Kim, M., Kobayashi, M., Kato, H. & Kakihana, M. A Highly Luminous $\text{LiCaPO}_4:\text{Eu}$ Phosphor Synthesized by a Solution Method Employing a Water-Soluble Phosphate Ester. *Optics & Photonics Journal* **3**, 13–18 (2013).
- Jiao, M. *et al.* Tunable Blue-Green-Emitting $\text{Ba}_3\text{LaNa}(\text{PO}_4)_3\text{F}:\text{Eu}^{2+}, \text{Tb}^{3+}$ Phosphor with Energy Transfer for Near-UV White LEDs. *Inorganic Chemistry* **52**, 10340–10346 (2013).
- Xin, S. & Zhu, G. Enhanced luminescence and abnormal thermal quenching behaviour investigation of $\text{BaHfSi}_3\text{O}_9:\text{Eu}^{2+}$ blue phosphor co-doped with $\text{La}^{3+}-\text{Sc}^{3+}$ ion pairs. *Rsc Advances* **6**, 41755–41760 (2016).

14. Zheng, Y. *et al.* Synthesis, structure and luminescent properties of a new blue-green-emitting garnet phosphor $\text{Ca}_2\text{LuScZrAl}_2\text{GeO}_{12}:\text{Ce}^{3+}$. *Rsc Advances* **6** (2016).
15. Ding, X., Zhu, G., Geng, W., Wang, Q. & Wang, Y. Highly efficient cyan-emitting garnet $\text{Ca}_3\text{Hf}_2\text{SiAl}_2\text{O}_{12}:\text{xCe}^{3+}$ phosphor for solid state white lighting. *Cryst Eng Comm* **17**, 3235–3242, <https://doi.org/10.1039/c5ce00020c> (2015).
16. Zhong, J. *et al.* Synthesis, Structure and Luminescence Properties of New Blue-Green-Emitting Garnet-Type $\text{Ca}_3\text{Zr}_2\text{SiGa}_2\text{O}_{12}:\text{Ce}^{3+}$ Phosphor for Near-UV Pumped White-LEDs. *Rsc Advances* **6**, 2155–2161 (2015).
17. Yu, R. *et al.* A new blue-emitting phosphor of Ce^{3+} -activated $\text{CaLaGa}_3\text{S}_6\text{O}$ for white-light-emitting diodes. *Chemical Physics Letters* **453**, 197–201 (2008).
18. Xia, Z., Du, H., Sun, J., Chen, D. & Wang, X. A novel blue-emitting $\text{Ca}_2\text{B}_5\text{O}_9\text{Br}:\text{Eu}^{2+}$ phosphor prepared by a microwave calcination route. *Materials Chemistry & Physics* **119**, 7–10 (2010).
19. Kim, Y. H. *et al.* A zero-thermal-quenching phosphor. *Nature Materials* **16**, 543 (2017).
20. Young & Olga. Magnetic properties of two geometrically frustrated compounds: SrHo_2O_4 and SrGd_2O_4 . *University of Warwick* (2013).
21. Petrenko, O. A. *et al.* Low-temperature magnetic ordering in SrEr_2O_4 . *Phys. rev. b* **78**, 2599–2604 (2008).
22. Karunadasa, H. *et al.* Honeycombs of triangles and magnetic frustration in SrL_2O_4 (L = Gd, Dy, Ho, Er, Tm, and Yb). *Phys. rev. b* **71**, 144414.144411–144414.144418 (2005).
23. Zhou, L., Shi, J. & Gong, M. Synthesis and photoluminescence properties of $\text{SrLu}_{\{2\}}\text{O}_{\{4\}}:\text{Eu}^{\{3+\}}$ superfine phosphor. *Materials Research Bulletin* **40** (2005).
24. Singh, J., Manam, J., Kumari, P. & Jana, S. Investigation of Thermal Stability of Red Emitting $\text{SrGd}_2(1-x)\text{Eu}_2\text{xO}_4$ Phosphors for Lighting and Display Applications. *Journal of Nano- and Electronic Physics* **9**, 03029–03021–03029–03024 (2017).
25. Kim, K. H., Kang, E. H., Kang, B. K., Kim, K. P. & Hong, S. H. Synthesis of $\text{SrLu}_2\text{O}_4:\text{Eu}^{2+}$ red phosphors and their photoluminescence properties. *Journal of Luminescence* **183**, 13–16 (2017).
26. Qin, X., Liu, X., Huang, W., Bettinelli, M. & Liu, X. Lanthanide-activated phosphors based on 4f–5d optical transitions: theoretical and experimental aspects. *Chemical reviews* **117**, 4488–4527 (2017).
27. Hermus, M., Phan, P.-C., Duke, A. C. & Brgoch, J. Tunable Optical Properties and Increased Thermal Quenching in the Blue-Emitting Phosphor Series: $\text{Ba}_2(\text{Y}_{1-x}\text{Lu}_x)_5\text{B}_5\text{O}_{17}:\text{Ce}^{3+}$ ($x=0-1$). *Chemistry of Materials* **29**, 5267–5275 (2017).
28. Blasse, G. Energy Transfer in Oxidic Phosphors. *Physics Letters A* **28**, 444–445 (1968).
29. Li, G., Fan, Y., Guo, H. & Wang, Y. Synthesis, structure and photoluminescence properties of Ce^{3+} -doped SrSc_2O_4 : a new scandate green-emitting phosphor with blue excitation. *New Journal of Chemistry* **41**, 5565–5571 (2017).
30. Uitert, L. G. V. Energy transfer between rare earth ions in tungstates. *Journal of Luminescence* **44**, 3514–3522 (1966).
31. Bhushan, S. & Chukichev, M. V. Temperature dependent studies of cathodoluminescence of green band of ZnO crystals. *Journal of Materials Science Letters* **7**, 319–321 (1988).
32. Im, W. B., Fellows, N. N., Denbaars, S. P. & Seshadri, R. $\text{La}_{1-x}\text{-x}0.025\text{Ce}0.025\text{Sr}_2+\text{xAl}_{1-x}\text{SixO}_5$ solid solutions as tunable yellow phosphors for solid state white lighting. *Journal of Materials Chemistry* **19**, 1325–1330 (2009).
33. Li, K., Shang, M., Lian, H. & Lin, J. Photoluminescence properties of efficient blue-emitting phosphor $\alpha\text{-Ca}_{1.65}\text{Sr}_0.35\text{SiO}_4:\text{Ce}^{3+}$: color tuning via the substitutions of Si by Al/Ga/B. *Inorganic chemistry* **54**, 7992–8002 (2015).
34. Ding, X., Zhu, G., Geng, W., Mikami, M. & Wang, Y. Novel blue and green phosphors obtained from $\text{K}_2\text{ZrSi}_3\text{O}_9:\text{Eu}^{2+}$ compounds with different charge compensation ions for LEDs under near-UV excitation. *Journal of Materials Chemistry C* **3**, 6676–6685 (2015).
35. Yan, C. *et al.* $\text{YSr}_2\text{Si}_4\text{N}_6\text{C}:\text{Ce}^{3+}$ • A Broad Cyan-Emitting Phosphor To Weaken the Cyan Cavity in Full-Spectrum White Light-Emitting Diodes. *Inorganic chemistry* **56**, 11087–11095 (2017).
36. Liu, Y. *et al.* $\text{Ba}_9\text{Lu}_2\text{Si}_6\text{O}_{24}:\text{Ce}^{3+}$: An Efficient Green Phosphor with High Thermal and Radiation Stability for Solid-State Lighting. *Advanced Optical Materials* **3**, 1096–1101, <https://doi.org/10.1002/adom.201500078> (2015).

Acknowledgements

This work was partially supported by National Key R&D Program of China (Grant Nos 2016YFB0701003, 2016YFB0400605, 2017YFB0403104), National Natural Science Foundation of China (Grant Nos 51772286, 51402284 and 11604330), Natural Science Foundation of Jilin province (Grant Nos 20150520022JH and 20160520171JH), and the prior sci-tech program of innovation and entrepreneurship of oversea Chinese talent of Jilin province.

Author Contributions

S.Z. and Z.D.H. conceived the idea, designed the experiment and co-wrote the manuscript. S.Z. and H.J.W. synthesized the phosphor and X.Z. fabricated the white LEDs. H.F.Z. analyzed the XRD patterns of the phosphors. Y.S.L. and L.G.Z. recorded the PL and PLE emissions of the phosphors. G.H.P. took photographs of phosphors using a fluorescence microscopy. L.L.Z. recorded and analyzed the FL emission of the white LEDs. All the authors discussed the results and commented on the manuscript. The whole work was carried out under the guidance of Z.D.H. and J.H.Z.

Additional Information

Supplementary information accompanies this paper at <https://doi.org/10.1038/s41598-018-28834-8>.

Competing Interests: The authors declare no competing interests.

Publisher's note: Springer Nature remains neutral with regard to jurisdictional claims in published maps and institutional affiliations.



Open Access This article is licensed under a Creative Commons Attribution 4.0 International License, which permits use, sharing, adaptation, distribution and reproduction in any medium or format, as long as you give appropriate credit to the original author(s) and the source, provide a link to the Creative Commons license, and indicate if changes were made. The images or other third party material in this article are included in the article's Creative Commons license, unless indicated otherwise in a credit line to the material. If material is not included in the article's Creative Commons license and your intended use is not permitted by statutory regulation or exceeds the permitted use, you will need to obtain permission directly from the copyright holder. To view a copy of this license, visit <http://creativecommons.org/licenses/by/4.0/>.

© The Author(s) 2018